INTERNATIONAL JOURNAL OF ROBUST AND NONLINEAR CONTROL
Int. J. Robust Nonlinear Control 2007; **00**:1–6 *Prepared using* rncauth.cls *[Version: 2002/11/11 v1.00]*

A Hybrid Model Predictive Control Approach to the Direct Torque Control Problem of Induction Motors

Georgios Papafotiou*, Tobias Geyer and Manfred Morari

Automatic Control Laboratory, ETH Zurich, CH–8092 Zurich, Switzerland

SUMMARY

Direct Torque Control (DTC) is a state of the art control methodology for electric motor drives which features favorable control performance and implementation properties. In DTC, the core of the control system is the inverter switching table, and any efforts to enhance the system's performance aim at improving its design. This issue is addressed in this paper, where we propose a new design procedure for the DTC problem. The DTC drive, comprising a two- or three-level dc-link inverter driving a three-phase induction motor, is modelled in the hybrid Mixed Logical Dynamical (MLD) framework, and a constrained finite time optimal control problem is set up and solved over a receding horizon using Model Predictive Control (MPC). Simulation results are provided and compared to the current industrial standard demonstrating the potential for notable performance improvements. Copyright © 2007 John Wiley & Sons, Ltd.

KEY WORDS: Model Predictive Control; Hybrid Systems; Induction Motor Drives; Direct Torque Control

1. INTRODUCTION

During the last decades, the development of power semiconductor devices has enabled the increased use of adjustable speed induction motor drives in a variety of applications. In these systems, DC-AC inverters are used to drive induction motors as variable frequency three-phase voltage or current sources. One of the various methods that are used for controlling the motor's torque and speed is Direct Torque Control (DTC), first introduced in 1985 by Takahashi and Noguchi [1]. Nowadays it is a well established industrial standard for induction motor drives [2].

The basic principle of DTC is to exploit the fast stator flux dynamics and to manipulate the stator flux vector such that the desired torque is produced. This is achieved by choosing an inverter switch combination that drives the stator flux vector to the desired position by directly applying the appropriate voltages to the motor windings. This choice is made usually with a sampling time $T_s = 25\,\mu$s using a pre-designed switching table that, depending on the

*Correspondence to: ABB Corporate Research, CH–5405 Baden-Dättwil, Switzerland (author's current affiliation)
†T. Geyer is currently with GE Global Research, Munich, Germany.

Copyright © 2007 John Wiley & Sons, Ltd.
Received 31 August 2006
Revised 21 February 2007

application, addresses a number of different control objectives. These primarily concern the induction motor - more specifically, the stator flux and the electromagnetic torque need to be kept within pre-specified hysteresis bounds around their references. In high power applications, where three-level neutral-point clamped inverters are used, the control objectives are extended to the inverter, and include the minimization of the average switching frequency and the balancing of the inverter's neutral point potential around zero.

The reasons that have motivated the use of DTC are the performance benefits it features, since the dynamic responses achieved in terms of torque are rapid and accurate throughout the whole operating range of the machine. On the other hand, its basic disadvantages are the high current and torque ripple, and the fact that the average inverter switching frequency is not directly controllable [3]. For addressing these issues, several different approaches have been proposed in the literature [4, 5], which mainly aim at improving the design of the switching table. Although these methods are well suited for two-level inverters, their extension to more complex problems featuring a larger number of available choices for the manipulated variables remains a difficult task [6].

The main reason for this difficulty is the fact that the DTC drive constitutes a hybrid system, i.e. a system incorporating both continuous and discrete dynamics - in particular discrete-valued manipulated variables. Additionally, constraints on states, inputs and outputs are present imposing further complications on the controller design, since the underlying mathematical problems are intrinsically complex and hard to solve. The main purpose of this paper is to investigate the potential benefits, in terms of performance and control design flexibility and extendability, that can be brought by employing model-based predictive control methodologies for hybrid systems as a solution approach for the DTC problem.

As shown in [7], the research community has recently started to consider predictive control schemes as a way of introducing performance improvements in induction (and synchronous) motor drives. Even though DTC itself can be interpreted as a predictive control strategy, it lacks the fundamental notions of a prediction model and a cost function; such elements are present in the more recent approaches [9], [10], and [11]. However, these schemes still differ in several aspects from the approach that will be presented in this paper. More specifically, (i) the prediction horizon is set to one, and there is no mention of a possible use of a larger (control) horizon combined with a receding horizon policy, (ii) the control problem is formulated as a reference tracking problem, and there are no hysteresis bounds on the controlled variables, (iii) the control objectives do not include the minimization of the switching frequency of the inverter, resulting to a simpler control problem, (iv) only two-level inverters are considered, and (v) linear (or locally linearized) models, which do not adequately capture the hybrid nature of the problem, are used as prediction models.

In this paper, a theoretical investigation of the DTC problem of three-phase induction motors is presented. Our goal is to investigate the existing potential for performance improvement in the currently used industrial DTC schemes, by employing hybrid modelling and optimal control techniques. Specifically, the DTC drive is modelled as a hybrid system where emphasis is given to the fast stator flux dynamics and the inverter switch positions are represented by integer variables. Nonlinearities are approximated by piecewise affine (PWA) functions, and the complete system including constraints is described in the *Mixed Logical Dynamical* (MLD) framework [12]. Based on the derived hybrid model, a constrained finite time optimal control problem over a receding horizon is set up and solved. The control strategy used is *Model Predictive Control* (MPC) [13], which is well suited for the optimal control of hybrid systems

Copyright © 2007 John Wiley & Sons, Ltd.

described in the MLD framework [14]. We will refer to this approach as *Optimal DTC*.

As the computation times needed for solving the optimal control problem online are well beyond the $25\,\mu$s sampling time of DTC, the proposed controller cannot be directly implemented. A possible way to overcome this obstacle is the calculation of the explicit state-feedback control law [15] by pre-computing offline the solution to the optimal control problem for the whole state-space using Dynamic Programming and multi-parametric programming. The resulting control law is a PWA state-feedback control law defined over a polyhedral partition of the state-space which can be stored in a look-up table. In this paper, we present the derivation and explore the complexity of such an explicit controller for the case of the two-level inverter.

The design procedure is demonstrated by applying the proposed approach to two cases, namely to DTC drives featuring a two- and a three-level inverter. In both cases, the design procedure remains essentially the same, and the extension to other inverter topologies with more degrees of freedom (like 5-level inverters) is straightforward. Concerning the potential performance improvements, we focus on the case of the three-level inverter considering ABB's ACS6000 DTC drive [16] containing a squirrel-cage rotor induction motor and a three-level neutral-point clamped dc-link inverter. The performance of the Optimal DTC scheme is evaluated through simulations and compared with ABB's DTC strategy showing a performance improvement in terms of a reduction of the switching frequency in the range of 20 %.

The paper is organized in the following way. Starting in Section 2 with basic terminology and the physical model of the DTC drive, Section 3 details the derivation of a low-complexity hybrid model that is used as internal prediction model for the optimal control problem formulated in Section 4, where we also compute the explicit state-feedback control law for a DTC drive with a two-level inverter. Simulation results for all considered cases are given in Section 5 using the above mentioned detailed ABB model of the drive. Finally, Section 6 concludes the paper with a summary and an outlook.

Throughout the paper, we will use the normalized time scale t with one time unit corresponding to $1/\omega_b$ seconds, where ω_b is the base angular velocity used to calculate the inductive reactances of the motor. Additionally, we will use $x(t)$, $t \in \mathbb{R}$, to denote continuous-time variables, and $x(k)$, $k \in \mathbb{N}$, to denote discrete-time variables with the sampling time $T_s = 25\,\mu$s. The state estimation of the motor was performed by an observer designed and provided by ABB, a detailed description of which is beyond the scope of this paper and has not been included.

2. MODELLING PRELIMINARIES

2.1. The dq0 Reference Frame

For the modelling of the DTC drive, all variables are transformed from the three-phase system (abc) to an orthogonal dq0 reference frame with a direct (d), a quadrature (q) and a zero (0) axis, that can be either stationary or rotating. Details regarding reference frame theory can be found in the relevant literature [17]. For the needs of this paper, the transformation of a vector $\boldsymbol{\xi}_{abc} = [\xi_a\ \xi_b\ \xi_c]^T$ from the three-phase system to the vector $\boldsymbol{\xi}_{dq0} = [\xi_d\ \xi_q\ \xi_0]^T$ in the dq0 frame is carried out through [17]

$$\boldsymbol{\xi}_{dq0} = \mathbf{P}(\varphi)\boldsymbol{\xi}_{abc}\,, \tag{1}$$

Copyright © 2007 John Wiley & Sons, Ltd.

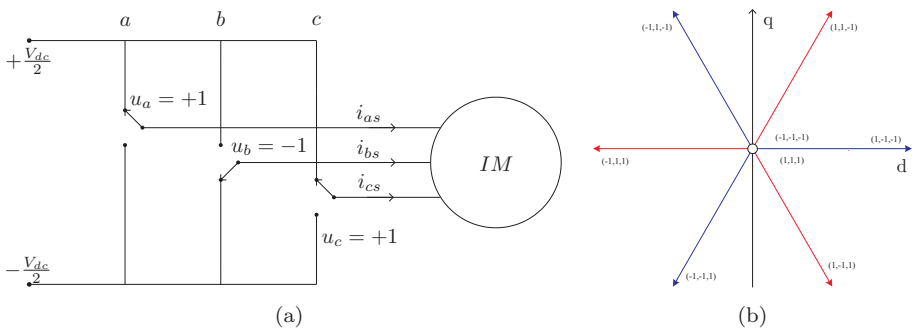

Figure 1: The equivalent representation of a three-phase two-level inverter driving an induction motor, and the voltage vectors produced by a two-level inverter on the dq plane, together with the corresponding values of the integer variables (switch positions)

where φ is the angle between the a-axis of the three-phase system and the d-axis of the reference frame, and

$$\mathbf{P}(\varphi) = \sqrt{\frac{2}{3}} \begin{bmatrix} \cos\varphi & \cos(\varphi - \frac{2\pi}{3}) & \cos(\varphi + \frac{2\pi}{3}) \\ -\sin\varphi & -\sin(\varphi - \frac{2\pi}{3}) & -\sin(\varphi + \frac{2\pi}{3}) \\ \frac{\sqrt{2}}{2} & \frac{\sqrt{2}}{2} & \frac{\sqrt{2}}{2} \end{bmatrix}. \tag{2}$$

If the frame is rotating with the angular speed ω_{fr}, then $\varphi = \omega_{fr}t + \varphi_0$ with φ_0 denoting the initial angle; otherwise, if the frame is stationary, φ is time-invariant. Note that the selected transformation matrix is orthonormal, i.e.

$$\mathbf{P}(\varphi)\mathbf{P}^T(\varphi) = \mathbf{I}. \tag{3}$$

2.2. Model of the Two-level Inverter

An equivalent representation of a three-phase two-level inverter driving an induction motor is shown in Fig. 1(a). The inverter can produce two different voltages $-\frac{V_{dc}}{2}, \frac{V_{dc}}{2}$ at each phase, where V_{dc} denotes the voltage of the dc-link. The switch positions of the inverter can be described using the integer variables u_a, u_b, $u_c \in \{-1, 1\}$, where each variable corresponds to one phase of the inverter, and the values $-1, 1$ correspond to the phase potentials $-\frac{V_{dc}}{2}, \frac{V_{dc}}{2}$, respectively. There are $2^3 = 8$ different vectors of the form $\mathbf{u}_{abc} = [u_a\ u_b\ u_c]^T$. Using (1) these vectors can be transformed in vectors in the dq0 frame shown in Fig. 1(b), where they are mapped into the two-dimensional dq plane.

2.3. Model of the Three-level Inverter

The equivalent representation of a three-phase three-level inverter driving an induction motor is shown in Fig. 2(a). The additional feature of the three-level inverter is that it can also produce a 0 phase voltage resulting in a total of three different possible voltages $-\frac{V_{dc}}{2}, 0, \frac{V_{dc}}{2}$ at each phase. The switch positions of the three-level inverter are now described using the integer variables $u_a, u_b, u_c \in \{-1, 0, 1\}$. As with the two-level inverter, each variable corresponds to one phase of the inverter, and the values $-1, 0, 1$ correspond to the phase potentials $-\frac{V_{dc}}{2}, 0, \frac{V_{dc}}{2}$, respectively. Similarly, there exist $3^3 = 27$ different vectors of the form $\mathbf{u}_{abc} = [u_a\ u_b\ u_c]^T$,

Copyright © 2007 John Wiley & Sons, Ltd.

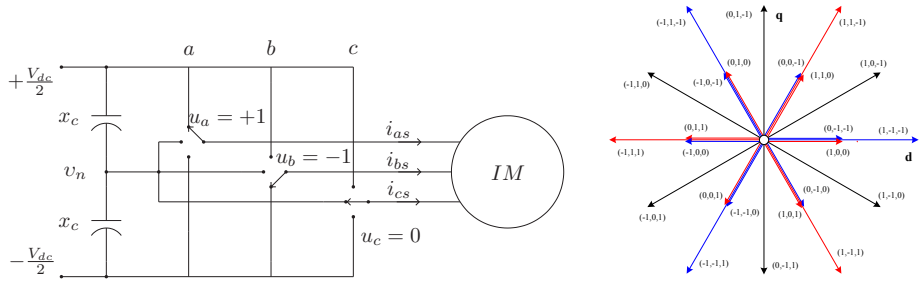

(a) (b)

Figure 2: The equivalent representation of a three-phase three-level inverter driving an induction motor, and the voltage vectors produced by a three-level inverter on the dq plane, together with the corresponding values of the integer variables (the three zero vectors $(+1, +1, +1)$, $(0, 0, 0)$ and $(-1, -1, -1)$ in the origin of the dq frame have been omitted due to the lack of space)

that can be transformed accordingly using (1), resulting in vectors in the dq0 frame shown in Fig. 2(b), where they are mapped into the dq plane.

Introducing v_n as a real state, the neutral point potential of the inverter (see fig. 2(a)) is described in continuous-time by

$$\dot{v}_n = -\frac{1}{2x_c}[(1 - |u_a|)i_{as} + (1 - |u_b|)i_{bs} + (1 - |u_c|)i_{cs}]\,, \tag{4}$$

with i_{as}, i_{bs}, i_{cs} being the phase stator currents and x_c one of the two symmetric capacitors of the dc-link. Taking into account that $i_{as} + i_{bs} + i_{cs} = 0$, and by transforming the vectors into the dq0 frame while taking advantage of (3), it is straightforward to derive

$$\dot{v}_n = \frac{1}{2x_c}\mathbf{u}^T_{|dq0|}\mathbf{i}_{s,dq0}\,, \tag{5}$$

where $\mathbf{i}_{s,dq0}$ is the stator current expressed in the dq0 frame and $\mathbf{u}_{|dq0|}$ is the transformation of the vector $|\mathbf{u}_{abc}| = [|u_a|\ |u_b|\ |u_c|]^T$. Note that the absolute value is defined componentwise. For more details about the nature of the neutral point potential and the related balancing problem see [18].

2.4. Model of the Induction Motor

The dynamics of the squirrel-cage rotor induction motor are modelled in the dq0 reference frame that is rotating synchronously with the rotor with the angular speed ω_r. The d- and q-components of the stator and rotor flux linkages per second ψ_{ds} , ψ_{qs} , ψ_{dr} and ψ_{qr}, respectively, and the rotor's rotational speed ω_r are used as state variables. The 0-axis components are neglected, since they do not contribute to the electromagnetic torque and are decoupled from the dynamics in the d- and q-axis. The input voltages v_{ds} and v_{qs} are the transformation of the voltages applied to the stator into the dq0 frame. The state equations are [17]

$$\dot{\boldsymbol{\psi}}_s = (\mathbf{F}_{sr} + \omega_r\mathbf{F}_\omega)\boldsymbol{\psi}_s + \mathbf{F}_{sm}\boldsymbol{\psi}_r + \boldsymbol{v}_s \tag{6a}$$

$$\dot{\boldsymbol{\psi}}_r = \mathbf{F}_{rm}\boldsymbol{\psi}_s + \mathbf{F}_{rs}\boldsymbol{\psi}_r \tag{6b}$$

$$\dot{\omega}_r = c_H\big(c_T\boldsymbol{\psi}_s \times \boldsymbol{\psi}_r - T_\ell\big)\,, \tag{6c}$$

Copyright © 2007 John Wiley & Sons, Ltd.

where $\boldsymbol{\psi}_s = \begin{bmatrix}\psi_{ds} & \psi_{qs}\end{bmatrix}^T$, $\boldsymbol{\psi}_r = \begin{bmatrix}\psi_{dr} & \psi_{qr}\end{bmatrix}^T$, and $\boldsymbol{v}_s = \begin{bmatrix}v_{ds} & v_{qs}\end{bmatrix}^T$. The matrices $\mathbf{F}_{sr}$, $\mathbf{F}_{sm}$, $\mathbf{F}_{rm}$, $\mathbf{F}_{rs}$, and $\mathbf{F}_{\omega}$ and the coefficients c_H and c_T are constants that depend on the motor parameters, while T_ℓ is the load torque of the motor. Finally, the electromagnetic torque is proportional to the external product of the two flux vectors

$$T_e = c_T \boldsymbol{\psi}_s \times \boldsymbol{\psi}_r = c_T(\psi_{qs}\psi_{dr} - \psi_{qr}\psi_{ds})\,. \tag{7}$$

For a more elaborate presentation of the induction motor's model see [17].

3. LOW COMPLEXITY DISCRETE-TIME MODELLING FOR CONTROLLER DESIGN

3.1. Symmetrical Properties of the System

The voltage vectors that can be produced by both a two- and a three-level inverter exhibit strong symmetrical properties in the dq plane. As can be seen from Figs. 1(b) and 2(b), a certain pattern is repeated with an angle spread of $\frac{\pi}{3}$. Defining such a pattern as a sector leads to the formation of six sectors. On the dq plane, rotating any sector by $\frac{\pi}{3}$ yields the vectors of the neighboring sector. This does not hold for the dq0 space, however, where the corresponding voltage vectors of neighboring sectors have opposite zero components. More formally, the voltage vectors of the μ sector can be used to produce the vectors of the ν sector through

$$\mathbf{u}_{dq0}^{(\nu)} = \mathbf{\Pi}^{\nu-\mu}\mathbf{u}_{dq0}^{(\mu)} \tag{8}$$

using the rotation matrix

$$\mathbf{\Pi} = \begin{bmatrix} \cos\frac{\pi}{3} & -\sin\frac{\pi}{3} & 0 \\ \sin\frac{\pi}{3} & \cos\frac{\pi}{3} & 0 \\ 0 & 0 & -1 \end{bmatrix}, \tag{9}$$

that takes the mapping of the zero component properly into account. This relationship can be also applied to the switch positions u_a, u_b and u_c given in the three-pase system (abc) by transforming the quantities to the dq0 reference frame, rotating them there from the μ to the ν sector, and transforming them subsequently back.

$$\mathbf{u}_{abc}^{(\nu)} = \mathbf{P}(\varphi)^{-1}\ \mathbf{\Pi}^{\nu-\mu}\ \mathbf{P}(\varphi)\mathbf{u}_{abc}^{(\mu)} \tag{10}$$

3.2. Stator Flux Dynamics Model

In order to derive a low-complexity model of the induction motor that is suitable for the optimal control problem formulation, two basic characteristics of DTC have to be taken into account. Firstly, the stator flux dynamics are significantly faster than the dynamics of the rotor flux and the rotational speed. Thus, the application of a certain voltage vector to the machine terminals has an immediate effect only on the stator flux, turning it rapidly to the position required by the torque demand, while the rotor speed ω_r and the *length* of the rotor flux vector remain constant during several control cycles.

The second characteristic is that the control objectives concerning the motor, namely the maintenance of the length of the stator flux vector and the electromagnetic torque within the specified bounds, are only affected by the relative (and not the absolute) position of the stator and rotor flux vectors. This is because the electromagnetic torque is the external product of

Copyright © 2007 John Wiley & Sons, Ltd.

these two vectors. Exploiting the symmetrical properties of the voltage vectors, it is sufficient to map the fluxes into the 0 sector, to solve the control problem in this sector, and to subsequently rotate the result back into the original sector yielding the voltage vector to be actually applied to the motor terminals.

To ease the modelling, we align the d-axis of the reference frame with the rotor flux vector. This is achieved by a rotation of the flux vectors that can be carried out in two stages. The first stage maps the problem into the 0 sector by rotating the flux vectors clockwise by an integer multiple of $\frac{\pi}{3}$, whereas the second stage is an anti-clockwise rotation of the reference frame by an angle $\varphi \in [0, \frac{\pi}{3}]$, that aligns the rotor flux vector with the d-axis of the reference frame. Assume that the rotor flux initially lies in sector ν. Rotating the fluxes by the angle $\vartheta = \frac{\nu\pi}{3} + \varphi$ yields the rotated flux vectors which are defined as

$$\boldsymbol{\psi}_s^{\vartheta} = \begin{bmatrix}\psi_{ds}^{\vartheta} & \psi_{qs}^{\vartheta}\end{bmatrix}^T, \quad \boldsymbol{\psi}_r^{\vartheta} = \begin{bmatrix}\psi_{dr}^{\vartheta} & \psi_{qr}^{\vartheta}\end{bmatrix}^T. \tag{11}$$

Given the fact that this rotation aligns the rotor flux vector with the d-axis of the rotating frame, and recalling the slow dynamics of the rotor flux vector, one introduces only a negligible error by assuming that ψ_{dr}^{ϑ} is constant and $\psi_{qr}^{\vartheta} = 0$ during several sampling intervals. Since the rotational speed dynamics are even slower, also ω_r remains constant.The stator flux dynamics can be described using a reference frame that is rotating synchronously with the rotor by a set of affine state equations

$$\dot{\boldsymbol{\psi}}_s^{\vartheta}(t) = (\mathbf{F}_{sr} + \omega_r \mathbf{F}_{\omega})\boldsymbol{\psi}_s^{\vartheta}(t) + \mathbf{F}_{sm}\boldsymbol{\psi}_r^{\vartheta} + \frac{V_{dc}}{2}\mathbf{P}(\varphi(k))\mathbf{u}_{abc}(t)\,, \tag{12}$$

that regard ω_r and ψ_{dr}^{ϑ} as parameters.

To derive the discrete-time mapping of the stator fluxes from the beginning of the sampling interval to its end, note that the voltage vector applied to the motor terminals remains constant within one sampling interval. The discrete-time model of the stator flux dynamics is then obtained by solving (12) from $t = kT_s$ to $t = (k+1)T_s$. Note that the matrix $\mathbf{P}(\varphi(k))$ performing the transformation of the inverter voltages into the rotating dq0 frame is time-varying. In particular, it depends on the angle φ

$$\varphi(k+1) = \varphi(k) + \omega_r T_s\,, \tag{13}$$

that captures the evolution of the rotating reference frame. The two outputs of the model are the electromagnetic torque and the length of the stator flux vector

$$T_e(k) = c_T \psi_{dr}^{\vartheta}\psi_{qs}^{\vartheta}(k)\,,\ \Psi_s(k) = \sqrt{(\psi_{ds}^{\vartheta}(k))^2 + (\psi_{qs}^{\vartheta}(k))^2}\,. \tag{14}$$

3.3. Discrete-time Model of the Three-level Inverter

The aspect of the neutral point potential must be addressed when using a three-level inverter and thus needs to be modelled properly. The neutral point potential that is described in continuous-time by (5) depends on $\mathbf{u}_{|dq0|}$ and $\mathbf{i}_{s,dq0}$. The d- and q-components of the stator current $\mathbf{i}_{s,dq0}$ are linear combinations of the d- and q-components of the stator and rotor flux vectors (see [17] for details and for the definition of the coefficients c_{rr} and c_m), and the

Copyright © 2007 John Wiley & Sons, Ltd.

0-component is always zero[†].

$$\mathbf{i}_{s,dq0} = \begin{bmatrix} c_{rr}\boldsymbol{\psi}_s^T - c_m\boldsymbol{\psi}_r^T & 0 \end{bmatrix}^T . \tag{15}$$

Recalling that the fluxes initially lie in the ν sector, and since the optimal control problem will be formulated and solved in the 0 sector, the obtained voltage vector has to be rotated counter-clockwise for ν sectors using (10), to yield the voltage vector that will be actually applied to the drive. For the componentwise absolute voltage vectors, the following non-trivial relation can be shown to hold

$$|\mathbf{u}_{abc}^{(\nu)}| = (-1)^\nu \, \mathbf{P}(\varphi)^{-1} \, \mathbf{\Pi}^\nu \, \mathbf{P}(\varphi) \, |\mathbf{u}_{abc}^{(0)}|, \tag{16}$$

stating that a voltage vector in the 0 sector and its corresponding vectors in the even sectors have the same componentwise absolute vectors. On the other hand, a voltage vector in the 0 sector and its equivalents in the odd sectors have opposite componentwise absolute vectors. Therefore, (5) can be written in discrete-time as

$$\upsilon_n(k+1) = \upsilon_n(k) + (-1)^\nu \frac{T_s}{2x_c} \, \mathbf{u}_{|dq0|}^T(k) \, \mathbf{i}_{s,dq0}(k), \tag{17}$$

where $(-1)^\nu$ accounts for property (16) of the componentwise absolute voltage vectors.

3.4. Mixed Logical Dynamical Framework

The existence of integer system inputs calls for appropriate modelling using hybrid methodologies. We employ the Mixed Logical Dynamical (MLD) framework, since it allows for convenient modelling using the HYbrid Systems DEscription Language Hysdel [19], and is well-suited for optimal control, namely Model Predictive Control (MPC). The general MLD form of a hybrid system is

$$\mathbf{x}(k+1) = \mathbf{A}\mathbf{x}(k) + \mathbf{B}_1\mathbf{u}(k) + \mathbf{B}_2\boldsymbol{\delta}(k) + \mathbf{B}_3\mathbf{z}(k) \tag{18a}$$

$$\mathbf{y}(k) = \mathbf{C}\mathbf{x}(k) + \mathbf{D}_1\mathbf{u}(k) + \mathbf{D}_2\boldsymbol{\delta}(k) + \mathbf{D}_3\mathbf{z}(k) \tag{18b}$$

$$\mathbf{E}_2\boldsymbol{\delta}(k) + \mathbf{E}_3\mathbf{z}(k) \leq \mathbf{E}_4\mathbf{x}(k) + \mathbf{E}_1\mathbf{u}(k) + \mathbf{E}_5 \, , \tag{18c}$$

where $k \in \mathbb{N}$ is the discrete time-instant, and $\mathbf{x} \in \mathbb{R}^{n_c} \times \{0,1\}^{n_\ell}$ denotes the states, $\mathbf{u} \in \mathbb{R}^{m_c} \times \{0,1\}^{m_\ell}$ the inputs and $\mathbf{y} \in \mathbb{R}^{p_c} \times \{0,1\}^{p_\ell}$ the outputs, with both real and binary components. Furthermore, $\boldsymbol{\delta} \in \{0,1\}^{r_\ell}$ and $\mathbf{z} \in \mathbb{R}^{r_c}$ represent binary and auxiliary continuous variables, respectively. For details on the MLD framework, the reader is referred to [12].

3.5. Hybrid Model of the DTC Drive with a Two-level Inverter

The overall MLD model of the DTC drive includes the two submodels of the induction motor and the two-level inverter. The motor state equations of the stator flux given in (12) have two states. A third state is needed to account for the rotating reference frame. Rather than introducing $\varphi(k)$, we choose $\cos(\varphi(k))$ as third state as this proves to be beneficial in terms of the model complexity as detailed below. Rewriting (13), the corresponding state equation is

$$\alpha(k+1) = \cos(\omega_r T_s)\alpha(k) - \sin(\omega_r T_s)\beta(k) \, , \tag{19}$$

[†]This follows from (1), taking into account that $i_{as} + i_{bs} + i_{cs} = 0$.

Copyright © 2007 John Wiley & Sons, Ltd.

(a) Induction motor model

Nonlinear Function	Argument	Number of Regions
$(\psi_{ds}^{\vartheta})^2$	$\psi_{ds}^{\vartheta} \in [0.8, 1.5]$	5
$(\psi_{qs}^{\vartheta})^2$	$\psi_{qs}^{\vartheta} \in [0, 0.7]$	5
β	$\alpha \in [0.5, 1]$	4

(b) Three-level inverter model

Nonlinear Function	Arguments	Number of Regions
$u_{\lvert ds\rvert} \cdot i_{ds}$	$(u_{\lvert ds\rvert}, i_{ds}) \in [-0.85, 0.85] \times [0.1, 0.7]$	8
$u_{\lvert qs\rvert} \cdot i_{qs}$	$(u_{\lvert qs\rvert}, i_{qs}) \in [-0.85, 0.85] \times [0, 1.5]$	8

Table I: PWA approximations of nonlinearities used in the MLD model of the DTC drive

where $\alpha(k) = \cos(\varphi(k)),\ \beta(k) = \sin(\varphi(k))$. The overall state vector amounts to

$$\mathbf{x}(k) = \begin{bmatrix}\psi_{ds}^{\vartheta}(k) & \psi_{qs}^{\vartheta}(k) & \alpha(k)\end{bmatrix}^T . \tag{20}$$

The model outputs are the electromagnetic torque T_e and the length of the stator flux vector Ψ_s yielding the output vector $\mathbf{y}(k) = \begin{bmatrix}T_e(k) & \Psi_s(k)\end{bmatrix}^T$, while the model inputs are the integer variables u_a, u_b and u_c

$$\mathbf{u}(k) = \begin{bmatrix}u_a(k) & u_b(k) & u_c(k)\end{bmatrix}^T \in \{-1, 1\}^3 . \tag{21}$$

The model of the DTC drive contains several nonlinearities, namely the length of the stator flux vector and the matrix $\mathbf{P}(\varphi(k))$ (2) with the components $\sin(\varphi(k))$ and $\cos(\varphi(k))$. As the MLD framework does not allow for modelling general nonlinear functions, they need to be approximated by PWA functions. To account for the evolution of the rotating reference frame, it would be straightforward to introduce $\varphi(k)$ as a state and to use (13) to describe its evolution. This, however, would necessitate the approximation of $\sin(\varphi(k))$ and $\cos(\varphi(k))$ as a function of $\varphi(k)$. Instead, we choose $\alpha(k) = \cos(\varphi(k))$ as a state and approximate $\beta(k)$ as a function of $\alpha(k)$ thus avoiding the approximation of one nonlinearity.

Additionally, we use in the MLD model the squared length of the stator flux vector rather than its length, thus turning the nonlinearity (14) with two arguments into two nonlinearities with one argument each. This leads to a more accurate and less complex PWA approximation. Table I(a) summarizes the PWA approximations together with the function domains and the number of regions used. The domains cover the whole range of operation which is smaller than $[-1, 1]$ due to the rotation of the fluxes into the 0 sector, while the number of regions results from a trade-off between the required model accuracy and the increase in the model complexity. For the problem considered here, the maximum approximation error was chosen to be smaller than 1 %.

The above procedure yields an MLD system with 3 real states, 55 z-variables, 21 δ-variables and 225 inequality constraints. The derivation of the MLD system is performed by the compiler HYSDEL generating the matrices of the MLD system starting from a high-level description of the system. The matrices are not explicitly provided here due to space limitations, but are available from [20].

Copyright © 2007 John Wiley & Sons, Ltd.

3.6. Hybrid Model of the DTC Drive with a Three-level Inverter

For a DTC drive with a three-level inverter (17) is added as a state equation leading to the overall state vector

$$\mathbf{x}(k) = \begin{bmatrix}\psi_{ds}^{\vartheta}(k) & \psi_{qs}^{\vartheta}(k) & \alpha(k) & \upsilon_n(k)\end{bmatrix}^T . \tag{22}$$

The model outputs are augmented by the neutral point potential resulting in $\mathbf{y}(k) = \begin{bmatrix}T_e(k) & \Psi_s(k) & \upsilon_n(k)\end{bmatrix}^T$, and the model inputs are the integer variables u_a, u_b and u_c

$$\mathbf{u}(k) = \begin{bmatrix}u_a(k) & u_b(k) & u_c(k)\end{bmatrix}^T \in \{-1, 0, 1\}^3 . \tag{23}$$

The state equation (17) of the neutral point potential contains two multiplications which are approximated as summarized in Table I(b), where $\mathbf{u}_{|dq0|} = [u_{|ds|}, u_{|qs|}, u_{|0s|}]^T$ and $\mathbf{i}_{s,dq0} = [i_{ds}, i_{qs}, i_{0s}]^T$. As $i_{0s} = 0$, the third multiplication is always zero. As in the previous case, the function domains are chosen such that the whole range of operation is covered. As the neutral point potential does not need to be controlled with a high precision, a relatively large approximation error is tolerable. Therefore, a maximal approximation error of 5 % was chosen leading to eight regions. The above procedure yields an MLD system with 4 (real) states, 91 z-variables, 61 (integer) δ-variables and 477 inequality constraints, and the corresponding MLD matrices are available from [20].

4. OPTIMAL DIRECT TORQUE CONTROL

4.1. Control Problem

The most prominent control objective concerning the induction motor is to keep the electromechanical torque close to its reference, which is set either directly by the user or by an additional speed control loop based on a PI controller. In order to avoid the saturation or demagnetization of the motor, the amplitude of the stator flux has to be kept between certain pre-specified bounds around the reference which are in general time-invariant. The main control objective concerning the inverter is to minimize the average switching frequency. In the case of the three-level inverter, the control objectives are extended to keeping the neutral point potential of the inverter within certain limits around zero.

The physical setup, i.e. the inverter driving the induction motor with discrete voltage vectors, makes it impossible to regulate and keep the torque and the stator flux arbitrarily close to their reference with a finite switching frequency. At steady state, reducing the torque ripple can only be achieved by increasing the switching frequency and vice versa. This results in a fundamental trade-off between the amplitude of the torque ripple and the switching frequency. As the switch transitions lead to heat losses in the inverter, the maximal switching frequency is limited by the technology of the inverter. Thus, instead of trying to regulate the torque to its reference, this control objective is relaxed in DTC, and the controller rather aims at keeping the torque and the stator flux within certain bounds around their references.

4.2. Optimal Direct Torque Control

Our controller is based on constrained finite-time optimal control with a receding horizon policy, more specifically on MPC. In MPC, the current control input is obtained by solving at

Copyright © 2007 John Wiley & Sons, Ltd.

each sampling instant an open-loop constrained optimal control problem over a finite horizon using the current state of the plant as the initial state. The underlying optimization procedure yields an optimal control sequence that minimizes a given objective function. By only applying the first control input in this sequence and by recomputing the control sequence at the next sampling instant, a receding horizon policy is achieved. A major advantage of MPC is its ability to cope with hard constraints on manipulated variables, states and outputs. Furthermore, as introduced in [12], the MLD framework can be straightforwardly embedded in MPC allowing one to use hybrid models given in the MLD form as prediction models for MPC.

4.3. Controller Objectives

Next, we formulate the controller objectives which can be classified in three priority levels. The main objective is to keep the torque and the magnitude of the stator flux within the pre-specified bounds, and to also retain the neutral point potential within bounds that are typically symmetric around zero. As these bounds must not be (significantly) violated, we assign to them the highest priority, and express them in the objective function using soft constraints which reflect the bounds.

The control objective with secondary priority is to minimize the average switching frequency. This is approximated by minimizing the number of switch *transitions* within the prediction interval. Due to the limited length of the prediction interval, one needs to enforce that switch transitions are only performed if absolutely necessary, i.e. when refraining from switching would lead to a violation of the bounds on the controlled variables within one time-step. This is implemented by associating a time-decaying penalty with the switch transitions, where switch transitions within the first time-step of the prediction interval result in larger penalties then those that are far in the future.

In particular for short prediction intervals, for a given state, two or more control inputs may have the same associated costs according to the two penalty levels introduced above. In the presence of such ambiguities, the control input is preferable that moves some of the controlled variables closest to their references, in particular the stator flux and the neutral point potential. We account for that by adding a third, low priority penalty level on the deviation of the stator flux and the neutral point potential from their respective references. For the torque, however, it is preferable to take full advantage of the window width. Thus we refrain from adding such a penalty term to the torque.

4.4. Objective Function

Based on the controller objectives, we establish next the mathematical expression of the objective function, which comprises a number of cost expressions. The soft constraints on the upper and lower torque bounds $T_{e,max}$ and $T_{e,min}$, respectively, lead for the electromagnetic torque to the cost expression

$$\varepsilon_T(\ell) = \begin{cases} q_T(T_e(\ell) - T_{e,max}) & \text{if } T_e(\ell) \geq T_{e,max} \\ q_T(T_{e,min} - T_e(\ell)) & \text{if } T_e(\ell) \leq T_{e,min} \\ 0 & \text{else}\,, \end{cases} \tag{24}$$

where $q_T \gg 0$ is the weight on the soft constraints and ℓ is the discrete time instant within the prediction horizon. The cost expression for the length of the stator flux vector is defined similarly using the upper and lower flux bounds $\Psi_{s,max}$ and $\Psi_{s,min}$, respectively, with an

Copyright © 2007 John Wiley & Sons, Ltd.

additional term penalizing the deviation from the reference $\Psi_{s,ref}$

$$\varepsilon_\Psi(\ell) = \begin{cases} q_F(\Psi_s(\ell) - \Psi_{s,max}) & \text{if } \Psi_s(\ell) \geq \Psi_{s,max} \\ q_F(\Psi_{s,min} - \Psi_s(\ell)) & \text{if } \Psi_s(\ell) \leq \Psi_{s,min} \\ q_f|\Psi_s(\ell) - \Psi_{s,ref}| & \text{else}\,, \end{cases} \tag{25}$$

with the weights q_F and q_f, $q_F \gg q_f > 0$, on the soft constraints and on the deviation from the reference, respectively. The switch transitions are penalized using a time-varying weight $q_u(\ell) > 0$ and the 1-norm

$$\varepsilon_u(\ell) = q_u(\ell)\|\mathbf{u}(\ell) - \mathbf{u}(\ell-1)\|_1\,. \tag{26}$$

The above stated cost expressions are the same for the two- and the three-level inverter. For the three-level inverter, however, the penalty for the neutral point potential needs to be added. The cost $\varepsilon_\upsilon(k)$ is defined according to (25) with the respective bounds $\upsilon_{n,max}$ and $\upsilon_{n,min}$, the reference 0, and the weights q_N and q_n.

Finally, we define $\boldsymbol{\varepsilon} = [\varepsilon_u\ \varepsilon_T\ \varepsilon_\Psi]^T$ for the case of the two-level inverter and $\boldsymbol{\varepsilon} = [\varepsilon_u\ \varepsilon_T\ \varepsilon_\Psi\ \varepsilon_\upsilon]^T$ for the three-level inverter, and consider the objective function

$$J(\mathbf{x}(k), \mathbf{u}(k-1), \mathbf{U}(k)) = \sum_{\ell=0}^{N-1} \|\boldsymbol{\varepsilon}(k+\ell|k)\|_1\,,$$

which penalizes the predicted evolution of $\boldsymbol{\varepsilon}(k+\ell|k)$ over the finite horizon N using the 1-norm.

4.5. Constrained Finite Time Optimal Control Problem

The control input at time-instant k is then obtained by minimizing the objective function (27) over the finite sequence of control inputs $\mathbf{U}(k) = [(\mathbf{u}(k))^T, \ldots, (\mathbf{u}(k+N-1))^T]^T$ subject to the evolution of the MLD model and its mixed-integer linear inequality constraints, the integrality constraints on $\mathbf{U}(k)$ and the cost expressions (24)-(26). This amounts to the constrained finite time optimal control problem (CFTOC)

$$\mathbf{U}^*(k) = \arg\min_{\mathbf{U}(k)} J(\mathbf{x}(k), \mathbf{u}(k-1), \mathbf{U}(k)) \tag{27a}$$

$$\text{subj. to} \quad (18), (21), (24) - (26) \tag{27b}$$

yielding the sequence of optimal control inputs $\mathbf{U}^*(k) = [(\mathbf{u}^*(k))^T, \ldots, (\mathbf{u}^*(k+N-1))^T]^T$, of which only the first input $\mathbf{u}^*(k)$ is applied to the inverter. At the next sampling interval, k is set to $k+1$, a new state measurement (or estimate) is obtained, and the CFTOC problem is solved again over the shifted horizon according to the receding horizon policy. As we are using the 1-norm in all cost expressions, the CFTOC problem amounts to solving an *Mixed-Integer Linear Program*, for which efficient solvers exist.

The optimal control problem posed above is intended to capture the average switching frequency. Therefore, a long prediction interval is beneficial. However, the computational complexity explodes as the prediction interval is increased. To account for that, we propose to use a short prediction *horizon* N, while still capturing the behavior of the system over a longer time interval. This is achieved by using multiple-rate prediction models, finely sampling the prediction model with $25\,\mu$s only for the first steps in the horizon, but more coarsely with a multiple of $25\,\mu$s for steps further in the future, employing an approach similar to utilizing blocking control moves [21].

Copyright © 2007 John Wiley & Sons, Ltd.

(a) Rated Values

Induction Motor			
V	3300 V	I	356 A
P	1.587 MW	S	2 MVA
f	50 Hz	ω_r	596 rpm
Inverter			
V_{dc}	4294 V	I	500 A

(b) Parameters

Induction Motor			
r_s	0.0108 p.u.	r_r	0.0091 p.u.
x_{ls}	0.1493 p.u.	x_{lr}	0.1104 p.u.
x_m	2.3489 p.u.		
Inverter			
V_{dc}	1.5937 p.u.	x_c	4.3715 p.u.

Table II: Induction motor and inverter rated values and parameters

4.6. The Explicit State-Feedback Control Law

A possible solution to the problem of the large computation times occurring when solving the optimal control problem online is the pre-computation of the optimal state-feedback control law offline for all feasible states using the state vector as a parameter. The optimal control law can be obtained by using the algorithm described in [22], where the solution is generated by combining dynamic programming with multi-parametric programming and some basic polyhedral manipulations.

The resulting optimal state-feedback control law $\mathbf{u}^*(k)$ is a PWA function of the state $\mathbf{x}(k)$. More specifically, the state-space is partitioned into polyhedral sets and for each of these sets the optimal control law is given as an affine function of the state. In this case, as the CFTOC is also a function of the last control input, we need to extend [22] slightly by fixing $\mathbf{u}(k-1)$ to a feasible integer combination before solving (27). In particular, when solving the CFTOC problem explicitly, we will get as many state-feedback control laws and polyhedral partitions as we have feasible binary input combinations. For the two-level inverter, we therefore expect eight, for the three-level inverter 27 different controllers.

5. SIMULATION RESULTS

The simulation results presented in this section illustrate the performance of the Optimal DTC scheme for the two- and the three-level inverter, respectively. The parameter values used in the simulations are given in the Tables II(a) and II(b). In all graphs, the units are normalized and the time scaling is in ms.

5.1. Optimal DTC with a Two-level Inverter

For a DTC drive featuring a two-level inverter, the optimal control problem was solved for the objective function (27) using a prediction horizon of $N = 2$. Employing a single-rate prediction model, all steps were set equal to the usual DTC sampling time of $25\,\mu$s. According to the prioritization of the control objectives, the penalties on the soft constraints were chosen to be $q_T = q_F = 3000$ for the torque and stator flux. The switch transitions are penalized with $q_u(0) = 14$, exponentially decaying within the prediction horizon. The deviation of the stator flux from its reference is penalized with $q_f = 0.01$.

Initially, the motor is running with a speed of $\omega_r = 0.8$ p.u. under a load torque of $T_\ell = 0.1$ p.u., when a step in the torque reference $T_{e,ref}$ is applied from 0.1 p.u. to 0.8 p.u.. As the simulation results in Fig. 3 show, the torque response under Optimal DTC is rapid, while

Copyright © 2007 John Wiley & Sons, Ltd.

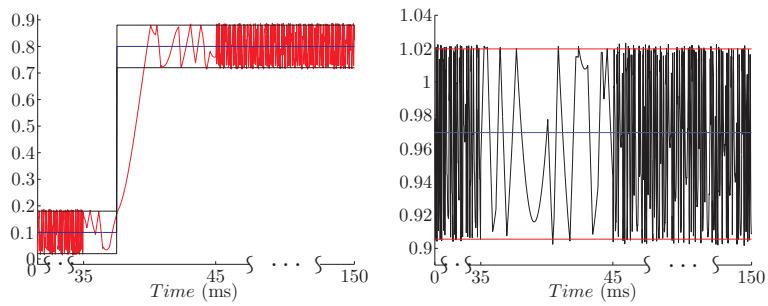

(a) Electromagnetic torque (b) Stator flux

Figure 3: Closed-loop simulation of the Optimal DTC scheme during a step change in the torque reference for a DTC drive with a two-level inverter

$\mathbf{u}(k-1)$	n_{org}	n_{mer}	reduc. [%]
$[-1\ -1\ -1]^T$	5246	709	86.5
$[-1\ -1\ +1]^T$	5325	753	87.6
$[-1\ +1\ -1]^T$	4737	486	89.7
$[-1\ +1\ +1]^T$	5292	625	88.2
$[+1\ -1\ -1]^T$	7019	930	86.8
$[+1\ -1\ +1]^T$	8512	880	90.0
$[+1\ +1\ -1]^T$	5425	631	88.4
$[+1\ +1\ +1]^T$	6295	617	90.2

Table III: Overview of the state-feedback control law for the DTC drive with a two-level inverter

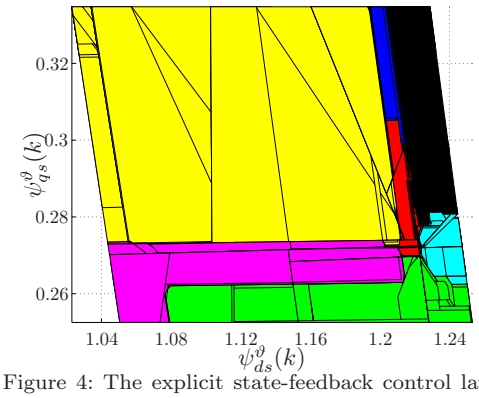

Figure 4: The explicit state-feedback control law for the DTC drive with a two-level inverter for $\mathbf{u}(k-1) = [+1\ -1\ -1]^T$ and $\alpha(k) = 0.95$, where the colors correspond to the control inputs $\mathbf{u}(k)$ ordered as in Table III: red, black, green, cyan, yellow, blue, magenta and red

the length of the stator flux remains within the specified bounds. Note that for the benefit of visualization, two different time scales were used, showing the step response between 35 ms and 45 ms in greater detail. The average switching frequency of the inverter was 515 Hz. The computation times required for the solution of the optimal control problem online at each time-step are in the range of 50 ms running CPLEX [23] on a 2.8 GHz Pentium PC.

To simplify the derivation of the explicit state-feedback control law, we only consider the case where the drive is operating at steady state at a fixed operating point. For this, we choose the operating point shown in Fig. 3 from 40 ms on, which is given by the speed $\omega_r = 0.8$ p.u., the load torque $T_\ell = 0.8$ p.u., and the torque bounds $T_{e,max} = 0.88$ p.u. and $T_{e,min} = 0.72$ p.u.. The reference of the stator flux is $\Psi_{s,ref} = 0.97$ p.u. and the corresponding bounds are $\Psi_{s,max} = 1.0198$ p.u. and $\Psi_{s,min} = 0.9025$ p.u.. The control problem formulation is the same as for the online optimization set-up.

The procedure described in Section 4.6 yields for each of the eight last control inputs (discrete states) a PWA state-feedback control law defined on the three-dimensional real state-space. Running subsequently the optimal merging algorithm [24] reduces the complexity of the control

Copyright © 2007 John Wiley & Sons, Ltd.

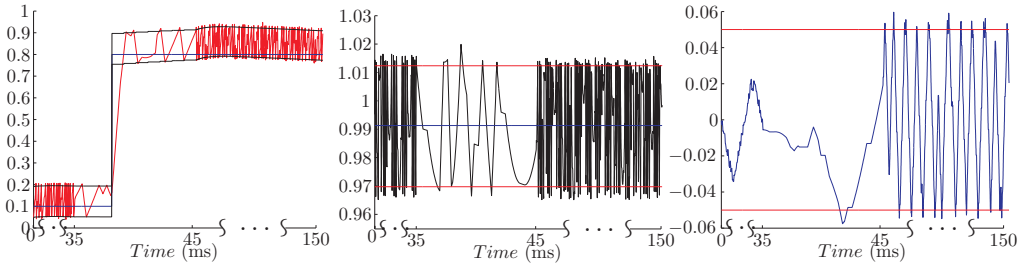

(a) Electromagnetic torque (b) Stator flux (c) Neutral point potential

Figure 5: Closed-loop simulation of the Optimal DTC scheme during a step change in the torque reference for a DTC drive with a three-level inverter

law, as the overview in Table III shows. For each last control input $\mathbf{u}(k-1)$, this table depicts the number of polyhedra of the original control law n_{org}, the number of polyhedra of the merged controller n_{mer}, the percentage reduction in the number of polyhedra, the computation time for the derivation of the explicit control law t_{expl} in hours, and the computation time for the optimal merging algorithm t_{mer} in hours. All computations where run on a 2.8 GHz Pentium with Linux using Matlab 6.5.

Figure 4 shows a two-dimensional cut through the polyhedral partition of the control law. For a geometrical interpretation of the result, the reader is referred to [8]. For completeness, we mention that choosing the same initial state at time 40 ms, both the on-line computation and the evaluation of the state-feedback control law yield the same closed-loop simulation results.

5.2. Optimal DTC with a Three-level Inverter

For the case of a DTC drive featuring a three-level inverter, the simulations were carried out using ABB's Matlab/Simulink model of the ACS6000 drive [16], where the look-up table with ABB's DTC strategy was replaced by a function solving at each time-step the optimal control problem online. The bounds for the torque and the stator flux depend on the operating point and are imposed by an outer control loop in the Matlab/Simulink model. A particularity of the specific inverter considered here is that restrictions on the switch transitions are present. These restrictions stem from technicalities regarding the construction of the inverter, and are easily taken into account in the Optimal DTC scheme by introducing additional constraints on the integer manipulated variables.

The optimal control problem was solved for the objective function (27) using a prediction horizon of $N = 3$. Using multiple rate prediction models, the first two steps were set equal to the sampling time of 25 μs and the remaining one was equal to 100 μs. The models were time-discretized accordingly. To allow for a comparison of ABB's DTC with the proposed Optimal DTC scheme, the penalties on the soft constraints were chosen such that the resulting ripples for the torque, flux and neutral point potential are the same. This led to $q_T = 800$ for the torque, $q_F = 700$ for the stator flux and $q_N = 4500$ for the neutral point potential. The switch transitions are penalized with $q_u(0) = 16$, exponentially decaying within the prediction horizon. The deviations from the references are penalized with $q_f = q_n = 0.04$ for the stator flux and the neutral point potential, respectively. The computation times required for the solution of the optimal control problem at each time-step were in the range of 100 ms running

Copyright © 2007 John Wiley & Sons, Ltd.

CPLEX [23] on a 2.8 GHz Pentium PC.

Initially, the motor is running with a speed of $\omega_r = 0.4$ p.u. under a load torque of $T_\ell = 0.1$ p.u., when a step in the torque reference $T_{e,ref}$ is applied from 0.1 p.u. to 0.8 p.u.. Fig. 5 depicts the closed-loop behavior of the torque, the stator flux and the neutral point potential under Optimal DTC. As can be seen, the Optimal DTC scheme achieves rapid dynamic responses, while the bounds imposed on the torque, stator flux and neutral point potential are only slightly violated. This degree of the violation of the bounds is a design parameter adjustable by the penalties on the soft constraints. Most important, the average switching frequency for Optimal DTC is only 196 Hz compared to the 256 Hz achieved by ABB's scheme for the same case. This improvement amounts to a reduction of the average switching frequency in the range of 20 %, which translates into an equivalent reduction of the switching losses.

6. CONCLUSIONS AND OUTLOOK

The scope of this paper is to investigate the potential improvements that can be achieved using optimal control methodologies for the hybrid control problem of DTC. The crucial ingredient for this is a hybrid model of the DTC drive that is of low complexity but yet sufficient accuracy, based on which the optimal control problem can be formulated and solved. The latter is tailored to the peculiarities of the DTC problem employing three different penalty levels, time-decaying penalty for the switch transitions and multiple rate prediction models. The proposed Optimal DTC approach is based on a systematic design procedure allowing one to easily adapt it to other inverter topologies. This is shown in the paper by applying the scheme to both the two- and the three-level inverter. Furthermore, this approach clearly demonstrates the potential for improving the performance of DTC with respect to state of the art industrial DTC look-up tables, as the comparison with ABB's ACS6000 drive emphasizes.

However, when solving the underlying optimization problem online to derive the control input, the corresponding computation times exceed the sampling time of DTC. Therefore, the proposed controller cannot be directly implemented and experimentally verified. One possible solution to this problem is the computation of the (explicit) state-feedback control law leading to an optimal look-up table. In this paper, for a DTC drive with a two-level inverter, this computation is carried out using dynamic programming, and the resulting state-feedback controller is analyzed in terms of its complexity. For the case of the three-level inverter, the combinatorial nature of the problem and the higher complexity of the model make the problem untractable using standard computational power at hand, and a different approach needs to be engineered. For this, preliminary results have been obtained featuring a complexity that is feasible for a practical implementation.

ACKNOWLEDGEMENTS

This work was supported by ABB Switzerland Ltd., and by the IST research project IST-2001-33520 *Control and Computation* of the EU. The authors would like to thank Christian Stulz, Pieder Jörg and Petri Schroderus of ABB ATDD, Turgi, Switzerland, and Andreas Poncet of ABB Corporate Research, Baden-Dättwil, Switzerland, for their continuous advice.

Copyright © 2007 John Wiley & Sons, Ltd.

REFERENCES

1. I. Takahashi and T. Noguchi. A new quick response and high efficiency control strategy for the induction motor. *IEEE Transactions on Industrial Applications* 1986; **22**(2):820–827.
2. P. Pohjalainen, P. Tiitinen, and J. Lulu. The next generation motor control method - direct torque control, DTC. *Proceedings of the European Power Electronics Chapter Symposium*; Lausanne, Switzerland, 1994. **1**:115–120.
3. D. Casadei, F. Profumo, G. Serra, and A. Tanni. FOC and DTC: Two viable schemes for induction motors torque control. *IEEE Transactions on Power Electronics* 2002; **17**(5):779–787.
4. D. Casadei, G. Serra, and A. Tanni. Implementation of a direct torque control algorithm for induction motors based on discrete space vector modulation. *IEEE Transactions on Power Electronics* 2000; **15**(4):769–777.
5. A. Purcell and P. Acarnley. Enhanced inverter switching for fast response direct torque control. *IEEE Transactions on Power Electronics* 2001; **16**(3):382–389.
6. C. Martins, X. Roboam, T. Meynard, and A. Carvalho. Switching frequency imposition and ripple reduction in DTC drives by using a multilevel converter. *IEEE Transactions on Power Electronics* 2002; **17**(2):286–297.
7. R. Kennel and A. Linder. Predictive control of inverter supplied electrical drives. *Proceedings of the 31st IEEE Power Electronics Specialists Conference*, Galway, Ireland, 2000; **2**:761–766.
8. T. Geyer. *Low complexity model predictive control in power electronis and power systems*. Diss. ETH No. 15953, Automatic Control Laboratory ETH Zurich, Zurich, 2005.
9. R. Kennel, A. Linder, and M. Linke. Generalized predictive control (GPC) – ready for use in drive applications? *Proceedings of the 32nd IEEE Power Electronics Specialists Conference*, Vancouver, Canada, 2001; **4**:1839–1844.
10. J. Rodriguez, J. Pontt, C. Silva, P. Cortes, U. Amman, and S. Rees. Predictive direct torque control of an induction machine. *Proceedins of the 11th IEEE Power Electronics and Motion Control Conference*, Riga, Latvia, 2004.
11. J. Retif, X. Lin-Shi, A. Llor, and F. Morand. New hybrid direct-torque control for a winding rotor synchronous machine. *Proceedings of the 35st IEEE Power Electronics Specialists Conference*, Aachen, Germany, 2004; **1**:1438–1442.
12. A. Bemporad and M. Morari. Control of systems integrating logic, dynamics and constraints. *Automatica* 1999; **35**(3):407–427.
13. J. Maciejowski. *Predictive Control*. Prentice Hall, 2002.
14. M. Tyler and M. Morari. Propositional logic in control and monitoring problems. *Automatica* 1999; **35**(4):565–582.
15. F. Borrelli, M. Baotić, A. Bemporad, and M. Morari. Dynamic programming for constrained optimal control of discrete-time linear hybrid systems. *Automatica* 2005; **41**(10):1709–1721.
16. ABB Asea Brown Boveri Ltd, Product webpage of ACS 6000.
Online document, www.abb.com/motors&drives [20 August 2006].
17. P. Krause. *Analysis of Electric Machinery*. McGraw-Hill: NY, 1986.
18. H. du Toit Mouton. Natural balancing of three-level neutral-point-clamped PWM inverters. *IEEE Transactions on Industrial Electronics* 2002; **49**(5):1017–1025.
19. F. Torrisi and A. Bemporad. Hysdel — a tool for generating computational hybrid models for analysis and synthesis problems. *IEEE Transactions on Control Systems Technology* 2004; **12**(2):235–249.
20. G. Papafotiou, T. Geyer and M. Morari. Optimal direct torque control of three-phase symmetric induction motors. *Tech. Rep. AUT03-07, Automatic Control Laboratory, ETH Zurich* 2003; http://control.ee.ethz.ch.
21. S. Qin and T. Badgwell. A survey of industrial model predictive control technology. *Control Engineering Practice* 2003; **11**(5):733–764.
22. M. Baotić, F. Christophersen, and M. Morari. A new algorithm for constrained finite time optimal control of hybrid systems with a linear performance index. *Proceedings of the European Control Conference*, Cambridge, UK, 2003.
23. ILOG, Inc. CPLEX 8.0 User Manual, Gentilly Cedex, France, 2002.
24. T. Geyer, F. Torrisi, and M. Morari. Optimal complexity reduction of piecewise affine models based on hyperplane arrangements. *Proceedings of the American Control Conference*, Boston, MA, 2004; **2**:1190–1195.

Copyright © 2007 John Wiley & Sons, Ltd.

Prepared using rncauth.cls